

Unenriched xylem water contribution during cellulose synthesis influenced by atmospheric demand governs the intra-annual tree-ring $\delta^{18}\text{O}$ signature

Elisabet Martínez-Sancho^{1,2} , Lucas A. Cernusak³ , Patrick Fonti¹ , Alessandro Gregori¹, Bastian Ullrich¹, Elisabeth Graf Pannatier¹ , Arthur Gessler¹ , Marco M. Lehmann¹ , Matthias Saurer¹  and Kerstin Treydte¹ 

¹Research Unit Forest Dynamics, Swiss Federal Institute for Forest Snow and Landscape Research WSL, Zürcherstrasse 111, Birmensdorf, 8903, Switzerland; ²Department of Biological Evolution, Ecology and Environmental Sciences, University of Barcelona, Diagonal 643, Barcelona, 08028, Spain; ³College of Science and Engineering, James Cook University, Cairns, QLD, 4878, Australia

Summary

Author for correspondence:
Elisabet Martínez-Sancho
Email: elisabet.martinez@wsl.ch

Received: 29 June 2023
Accepted: 16 August 2023

New Phytologist (2023)
doi: 10.1111/nph.19278

Key words: isotopic fractionation, mechanistic modeling, Péclet, p_{ex} , stable oxygen isotopes, tree rings, water, xylogenesis.

- The oxygen isotope composition ($\delta^{18}\text{O}$) of tree-ring cellulose is used to evaluate tree physiological responses to climate, but their interpretation is still limited due to the complexity of the isotope fractionation pathways.
- We assessed the relative contribution of seasonal needle and xylem water $\delta^{18}\text{O}$ variations to the intra-annual tree-ring cellulose $\delta^{18}\text{O}$ signature of larch trees at two sites with contrasting soil water availability in the Swiss Alps. We combined biweekly $\delta^{18}\text{O}$ measurements of soil water, needle water, and twig xylem water with intra-annual $\delta^{18}\text{O}$ measurements of tree-ring cellulose, xylogenesis analysis, and mechanistic and structural equation modeling.
- Intra-annual cellulose $\delta^{18}\text{O}$ values resembled source water $\delta^{18}\text{O}$ mean levels better than needle water $\delta^{18}\text{O}$. Large parts of the rings were formed under high proportional exchange with unenriched xylem water (p_{ex}). Maximum p_{ex} values were achieved in August and imprinted on sections at 50–75% of the ring. High p_{ex} values were associated with periods of high atmospheric evaporative demand (VPD). While VPD governed needle water $\delta^{18}\text{O}$ variability, we estimated a limited Péclet effect at both sites.
- Due to a variable p_{ex} , source water has a strong influence over large parts of the intra-annual tree-ring cellulose $\delta^{18}\text{O}$ variations, potentially masking signals coming from needle-level processes.

Introduction

The oxygen isotope ($\delta^{18}\text{O}$) composition of tree rings provides a powerful tool to evaluate tree physiological responses to their environments (McCarroll & Loader, 2004). Due to their natural link with water-related sources, tree-ring series of $\delta^{18}\text{O}$ has been strongly coupled with hydroclimatic information such as soil moisture (Hartl-Meier *et al.*, 2014), precipitation (Treydte *et al.*, 2006, 2007; Loader *et al.*, 2020), drought (Labuhn *et al.*, 2016; Büntgen *et al.*, 2021), and relative humidity (Wernicke *et al.*, 2015). Furthermore, $\delta^{18}\text{O}$ can be used to independently complement information from stable carbon isotopes to constrain stomatal conductance from tree physiological responses (i.e. dual-isotope approach, Scheidegger *et al.*, 2000; Grams *et al.*, 2007). However, crucial gaps in the mechanistic understanding of how physiological and climatic signals propagate into the tree-ring $\delta^{18}\text{O}$ signature are still unresolved and hinder straightforward interpretation of this tree-ring climate proxy due

to the complexity of the isotopic fractionations and oxygen atom exchange along the tree-internal pathway.

Indeed, the main processes playing a role in defining the final tree-ring $\delta^{18}\text{O}$ signature are located at source water variations, processes at the leaf level, and synthesis of wood constituents (Gessler *et al.*, 2014; Treydte *et al.*, 2014). The partitioning of these influences through the growing season and how climate conditions modify such partitioning are questions still to be answered in order to exploit the full potential of long tree-ring $\delta^{18}\text{O}$ series. The source water taken up by the roots and transported through the xylem to the leaves carries a specific signal composed of the precipitation $\delta^{18}\text{O}$ signature altered by evaporative ^{18}O enrichment of soil water and/or influenced by groundwater (Cernusak *et al.*, 2016). In the leaves, a substantial enrichment of the heavier isotope occurs at evaporative sites. This enriched water diffuses from the evaporative sites back into the leaf, with such diffusion opposed by convective transport toward the evaporative sites, resulting in mixing of enriched and

unenriched water in the leaf lamina, that is the Péclet effect (Farquhar & Lloyd, 1993). Although the Péclet effect is a theoretically sound concept and is essential for understanding how leaf water finally imprints the tree-ring $\delta^{18}\text{O}$ signature (Ferrio *et al.*, 2009), direct support for its relevance has been surprisingly hard to come by Loucos *et al.* (2015) and Roden *et al.* (2015).

Further fractionation steps occur during the production of sucrose at the leaf level and its conversion to cellulose within the stem. The first usually results in a temperature-dependent enrichment of *c.* 27‰ due to equilibrium with leaf water (Sternberg & DeNiro, 1983; Yakir & DeNiro, 1990). However, further exchange occurs with unenriched xylem (source) water during the sucrose-cellulose conversion within the stem. This proportion of oxygen exchange is termed p_{ex} and is determined to a large part by the rate of cycling of hexose phosphates through triose phosphate before incorporation into cellulose, which would expose more carbonyl oxygen to the xylem water before being incorporated into cellulose (Hill *et al.*, 1995; Waterhouse *et al.*, 2002). This means that a portion of carbonyl oxygen atoms (enriched sugars) is exchanged with unenriched xylem water, thus diluting the isotopic signal coming from the leaf water enrichment and subsequent biochemical processes at the leaf level. Although initial studies suggested that p_{ex} is a rather constant parameter (*c.* 0.42) regardless of environmental conditions and species-specific thresholds (Cernusak *et al.*, 2005), recent evidence points to a potentially seasonally varying value (e.g. Offermann *et al.*, 2011). The drivers of this unequal p_{ex} along the growing season are still unclear, but some studies have found associations with changes in aridity (Cheesman & Cernusak, 2016), and turnover time of the sucrose pool available for cellulose synthesis (Song *et al.*, 2014). Both mechanisms might interact with the rate of cycling of hexose phosphates through triose phosphate leading to differential levels of p_{ex} along the year. This fact adds further uncertainties related to the dilution of the $\delta^{18}\text{O}$ signature generated at the leaf level with the unenriched xylem water during cellulose formation (Ogée *et al.*, 2009) since xylem water influence may change throughout the year as modulated by environmental conditions and tree metabolism.

The strong knowledge of some of the processes and fractionation mechanisms of $\delta^{18}\text{O}$ along the tree pathway has allowed plant scientists to develop mechanistic models which mathematically describe the changes in the isotopic signals from water to sucrose and cellulose (Song *et al.*, 2022). For instance, mechanistic models focused on leaf water processes represent reasonably well the environmental drivers of leaf water $\delta^{18}\text{O}$. However, modeling cellulose $\delta^{18}\text{O}$ (Barbour & Farquhar, 2000; Roden *et al.*, 2000) is an additional challenge due to the complexity inherent to wood formation processes (Rathgeber *et al.*, 2016). Developing woody cells undergo several climate-sensitive phases before becoming stable and fully functional, including cell division, enlargement, and wall thickening. The cell wall thickening process is the main source of cellulose since the primary wall entails relatively low cellulose content (Cuny *et al.*, 2015; O'Neill & York, 2018). The timing and rates of cell wall formation are individual cell-based processes that are not constant along the growing season and are highly sensitive to environmental changes

(Deslauriers *et al.*, 2014). Therefore, $\delta^{18}\text{O}$ changes along sections of a tree ring (intra-ring) cannot directly be assigned to temporal windows (intra-annual) without accounting for a space-for-time conversion based on the radial position of the measured wood sections within a ring and the specific timing of formation of the cells within the same wood sections (Pérez-de-Lis *et al.*, 2021). Previous studies highlighted the importance of including information on intra-ring characteristics of tree-ring cell development to understand intra-seasonal tree-ring $\delta^{18}\text{O}$ variations (Belmecheri *et al.*, 2018; Szejner *et al.*, 2020), but only recent advances provide a framework to include heterogeneity in xylogenesis into intra-annual tree-ring studies (Pérez-de-Lis *et al.*, 2021; Martínez-Sancho *et al.*, 2022). The combination of specific information on cell kinetics with mechanistic isotope models has enormous potential to resolve key questions such as those related to the drivers of p_{ex} .

In this study, we aim to unravel the relative contribution of seasonal $\delta^{18}\text{O}$ variations in needle and xylem water to the intra-annual $\delta^{18}\text{O}$ values of tree-ring cellulose by (1) assessing the connection between isotopic changes in major parts of the tree-internal $\delta^{18}\text{O}$ pathway and (2) identifying the role of the different fractionation/exchange steps and their climatic and physiological drivers, specifically Péclet and p_{ex} . To do so, we analyzed intra-annual $\delta^{18}\text{O}$ data of xylem and needle water and tree-ring cellulose of seven larch trees (*Larix decidua* L.) at two sites with contrasting soil water availability during two growing seasons, statistically assessed the effects and interactions among the $\delta^{18}\text{O}$ signatures of the different tree tissues, and benchmarked the mechanistic models to understand the drivers of the main fractionations processes.

Materials and Methods

Study sites

We conducted our study at the tree-growth monitoring transect in the Lötschental (<https://www.wsl.ch/loetschental-monitoring>), an inner-alpine dry valley located in the Swiss Alps (Fig. 1a). We selected two sites with contrasting conditions of water availability located at a close distance at the valley bottom (46°23'40"N, 7°45'35"E) at an elevation of 1360 m above sea level (asl). The dry site is situated on a small rocky hill, which favors water drainage whereas the wet site is located near a small perennial stream (Fig. 1b). Environmental data, air temperature, and relative humidity were measured at the sites with a 15-min resolution during the study period (2012–2013) at 2 m aboveground (U23-002 HOBO Pro; Onset, Bourne, MA, USA). Soil volumetric water content was measured hourly at two soil depths between 10 and 70 cm depth (θ (%); EC-5; Decagon, Pullman, WA, USA). Vapor pressure deficit (VPD) was calculated as the difference between saturation vapor pressure and the actual vapor pressure. VPD was included in the characterization of the study sites to assess its effect on $\delta^{18}\text{O}$ variations due to its strong link with leaf water evaporative ^{18}O enrichment and transpiration.

Transpiration rates were obtained from 15-min resolution sap flux density (Fd, $\text{cm}^3 \text{m}^{-2} \text{h}^{-1}$) measurements using Granier's thermal dissipation probes. The Fd was calculated using the

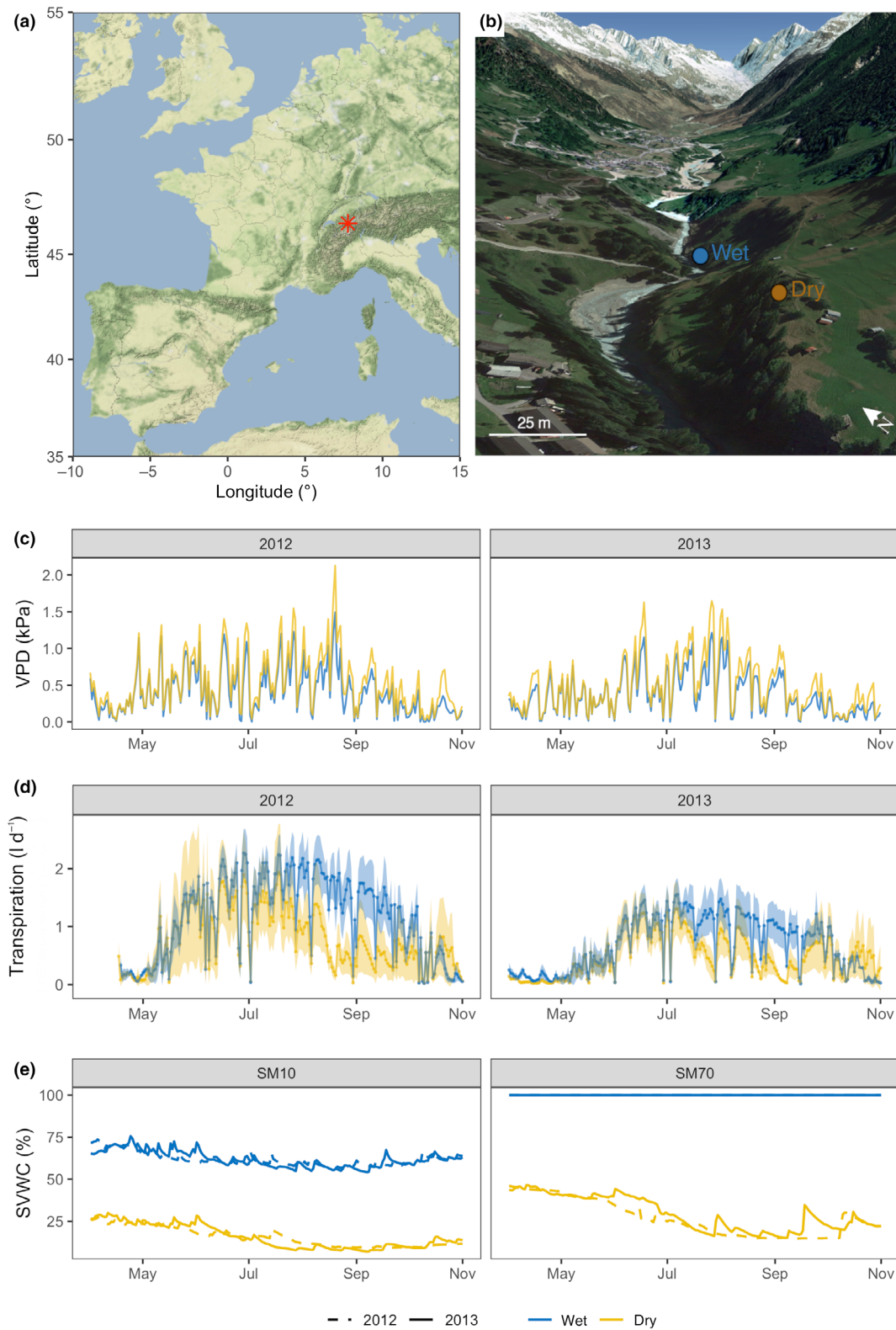


Fig. 1 Geographical location and climatic conditions of the sites during the study period. Geographical location of the two study sites in Switzerland (a) and within the Lötschental valley (b). VPD, vapor pressure deficit (c), mean diurnal tree transpiration (d), and SVWC, soil water content, at 10 and 70 cm depth (e) during the years 2012 and 2013. 3D Map data: Google, Maxar Technologies.

method described in Peters *et al.* (2018b), applying a species-specific calibration, dampening correction, and environment-dependent zero-flow conditions. Fd was multiplied by sapwood

area to obtain water flow to the crown (transpiration). Transpiration measurements were aggregated during daytime hours (06:00–22:00 h Central European Time).

Sampling of different waters and cellulose material

Weekly or biweekly sampling took place during the growing seasons (April to November) 2012–2013. Soil water was collected at 5 and 60 cm depth via tension lysimetry using glass suction plates and ceramic suction cups. Five replicates of soil water were collected per site, day and depth. The lysimeters were connected to 250-ml glass bottles and stored in an insulated and light-excluding box. A vacuum of *c.* 400 hPa was generated and renewed every 5 h to obtain a sample representative of conditions between the weekly samplings.

We selected a total of seven adult individuals of larch (*Larix decidua* L.) for sampling of needle and xylem water (four at the dry site and three at the wet; Supporting Information Fig. S1; Table S1). Tree selection at the wet site was determined by the trees' proximity to the perennial stream, resulting in a limited number of trees that met this criterion. Twigs 10–20 cm in length located in the sun-exposed part of the crown at a height between 2 and 5 m were collected for each tree, and the time of collection was noted. Needles and twig xylem (without bark) were separated and first stored in airtight closed glass tubes, transported to the laboratory on ice, and later kept in the freezer at -18°C . Needle and xylem water was extracted by cryogenic vacuum extraction (Ehleringer *et al.*, 2000). Extraction was under a vacuum of 0.03 hPa for at least 2 h where samples were heated to 80°C , and evaporated water was collected in U-tubes submerged in liquid nitrogen. These water extracts and the soil water samples were then equilibrated and analyzed for $\delta^{18}\text{O}$ at the Central Laboratory of the WSL with a Gas bench II combined with a Delta V Advantage mass spectrometer (Thermo Fisher Scientific Inc., Waltham, MA, USA) with a precision of $\pm 0.2\text{‰}$.

In 2020, increment cores of 1-cm diameter were collected at breast height from the same individuals. Samples for the intraring isotope analyses were obtained by cutting tangential sections of 50- μm thickness using a rotary microtome (Leica RM2245; Leica Biosystems, Nussloch, Germany) surrounded by a digital camera to guide the orientation of the cuts. Holocellulose extraction was performed for each sample (Boettger *et al.*, 2007), homogenized using an ultrasonic treatment (Laumer *et al.*, 2009), freeze-dried, and finally packed into silver capsules. Samples were then quantitatively converted to CO on a high-temperature TC/EA (1420°C ; Pyrocube, Elementar, Hanau, Germany) and $\delta^{18}\text{O}$ determined by IRMS (MAT253; Thermo, Bremen, Germany) with a precision better than 0.2‰. Both water and cellulose isotopic abundances are expressed relative to the international standard Vienna Standard Mean Ocean Water (VSMOW) using δ notation (‰).

Dynamics of cell wall formation

Information from cell formation and kinetics is crucial to assign a time window to each micro-section of a tree ring and its isotopic value (Pérez-de-Lis *et al.*, 2021; Martínez-Sancho *et al.*, 2022). Wood formation dynamics were assessed from four other representative larches located at the same study sites for the years 2012 and 2013. Microcores were biweekly collected using a Trephor

increment puncher (Rossi *et al.*, 2006). Laboratory procedures included embedding the microcores in paraffin with a HistoCore PEARL tissue processor (Leica Biosystems, Nussloch, Germany), cutting for microslide preparation using a rotary microtome, staining with a solution of Astra blue and Safranin, and digitalization with both bright and polarized light (Axio Scan.Z1; Zeiss). Cell counts of the different cell development phases, including cambial division, cell enlargement, cell wall formation (thickening and lignification), and maturation, provided the basis to later determine the cell kinetics. The timing (date of initiation and cessation) and duration (the number of days) of the phases (cambial, enlargement, wall thickening, and mature phases) for each cell in each ring were determined using generalized additive models with a quasi-Poisson distribution of the residuals (Wood, 2006; Cuny *et al.*, 2013; Pérez-de-Lis *et al.*, 2021; Notes S1). Quantitative wood anatomical measurements of each cell were obtained from digital images of the tree rings analyzed with ROXAS (Arx & Carrer, 2014). Cell radial diameter was calculated as the sum of the radial lumen area and double radial cell wall thickness. The R package RAPTOR (Peters *et al.*, 2018a) was used to assign each tracheid to its radial file and to obtain an average value for each position. The cell radial diameter provided us with the information necessary to assign the percentage of the ring that every cell was occupying in a radial profile (see procedure in Cuny *et al.*, 2019), which was then combined with the timing (date of initiation and cessation) and duration (the number of days) of the phases (cambial, enlargement, wall thickening, and mature phases) of each cell (Fig. S2).

Finally, the timing and duration that each tangential cut of the tree rings spent in the cell wall formation phase was identified by accounting for the percentage of the ring represented by each cut in combination with the above cell wall formation dynamics. This space-for-time conversion allowed us to translate the cell positions (analyzed as % of the ring width, intra-ring) into the corresponding time of cell formation for each cell developing phase (analyzed as days of the year, DOY, intra-annually; Fig. S3).

Quantification of relationships along the $\delta^{18}\text{O}$ pathway

Structural equation models (SEM) were applied to statistically assess the relations among $\delta^{18}\text{O}$ variations of the different pathway components as well as the effect of the most direct environmental and physiological mechanisms influencing $\delta^{18}\text{O}$ variations. SEMs examine linear causal relationships among variables, while being able to deal with the interdependence of variables and decompose total effects in direct and indirect types. We defined the pathway based on the current literature about abiotic and biotic processes affecting $\delta^{18}\text{O}$ fractionation (Treydte *et al.*, 2014). The influence of soil water $\delta^{18}\text{O}$ was only assessed at the wet site due to the above-mentioned data gaps at the dry site. Data from all the variables were time integrated by averaging values for the period when each tree-ring section was in the cell wall formation phase. Only periods with overlap between cell wall formation and available xylem and needle water $\delta^{18}\text{O}$ measurements were considered. The LAVAAN R package was used

for this analysis, running 1000 bootstrapped resamples with confidence intervals and *P*-values determined using the Bollen–Stine bootstrapping method (Rosseel, 2012). Finally, we used a comparative fit index (CFI), the standardized root mean square residual of approximation (RMSEA), to confirm the goodness of fit (Hooper *et al.*, 2008).

Mechanistic modeling: $\delta^{18}\text{O}$ needle water and cellulose

Needle water $\delta^{18}\text{O}$ values and variations were modeled and compared with observed needle water using the Craig–Gordon model (C–G model, Craig & Gordon, 1965):

$$\delta^{18}\text{O}_{\text{NW C-G}}(\text{‰}) = \delta^{18}\text{O}_{\text{XYL}} + \varepsilon_k + \varepsilon^+ + (\delta^{18}\text{O}_V - \delta^{18}\text{O}_{\text{XYL}} - \varepsilon_k) \frac{w_a}{w_i} \quad \text{Eqn 1}$$

where $\delta^{18}\text{O}_{\text{XYL}}$ is the isotopic composition of the xylem water, ε_k the kinetic fractionation for combined diffusion through the stomata and the boundary layer, $\delta^{18}\text{O}_V$ the isotopic composition of the water vapor in the air, and $\frac{w_a}{w_i}$ is the ratio of the water vapor mole fraction in the air relative to that in the intercellular air spaces, which is mainly driven by changes in relative humidity. The term ε^+ describes the isotope fractionation factor during liquid–vapor equilibrium of pure water, that depends on the temperature of the liquid–vapor interface, assumed here to be equal to bulk leaf temperature (*T*, in K; Majoube, 1971). It is expressed as:

$$\varepsilon^+ = \left[\exp\left(\frac{1173}{T^2} - \frac{0.4156}{T} - 0.0020667\right) - 1 \right] \times 1000 \quad \text{Eqn 2}$$

We estimated $\delta^{18}\text{O}_V$ as the difference between $\delta^{18}\text{O}_{\text{XYL}}$ (considered here as a source water) and ε^+ , assuming that water vapor is in equilibrium with source water (Foerstel & Huetzen, 1983).

The Péclet effect modifies the C–G model by considering the dilution of enriched water at the sites of evaporation by transpiration as:

$$\delta^{18}\text{O}_{\text{NW}}(\text{‰}) = \delta^{18}\text{O}_{\text{XYL}} + (\delta^{18}\text{O}_{\text{NW C-G}} - \delta^{18}\text{O}_{\text{XYL}}) \times \left(\frac{1 - e^{-\varphi}}{\varphi}\right) \quad \text{Eqn 3}$$

The Péclet number (φ) reflects the ratio between advection of unenriched water via the transpiration stream to back-diffusion of the enriched water (Farquhar & Lloyd, 1993), and it is calculated as:

$$\varphi = \frac{L E}{C D} \quad \text{Eqn 4}$$

where *L* is the effective path length (m) for the advective flow in the needle, *E* is the transpiration rate ($\text{mol m}^{-2} \text{s}^{-1}$), *C* is the molar density of water ($55.5 \times 10^3 \text{ mol m}^{-3}$), and *D* is the diffusivity of H_2^{18}O in water ($\text{m}^2 \text{s}^{-1}$). Details of the formulas and calculations are explained in Notes S2. The similarities of the observed values

and the outcome of both models (C–G and Péclet) were quantified by root mean square error (RMSE) and mean absolute error (MAE) of the needle water enrichment above xylem water. The predictive accuracy of the two models can be additionally evaluated by investigating the fractional difference between predicted and observed bulk needle water enrichment at the evaporation sites as described in Cernusak *et al.* (2016):

$$f = 1 - \Delta^{18}\text{O}_L / \Delta^{18}\text{O}_m \quad \text{Eqn 5}$$

where $\Delta^{18}\text{O}_L$ is the observed ^{18}O -enrichment above xylem water, calculated as $\Delta^{18}\text{O}_L = (\delta^{18}\text{O}_{\text{NW}} - \delta^{18}\text{O}_{\text{XYL}}) / (1 + (\delta^{18}\text{O}_{\text{XYL}} / 1000))$. For modeling of tree-ring cellulose $\delta^{18}\text{O}$, it needs to be considered that a fraction of the sugars that reflect the isotopic signal of the needle water will undergo an additional oxygen exchange with non-enriched water during cellulose biosynthesis (Sternberg *et al.*, 2006). This exchange of carbonyl oxygen with unenriched water is described by Roden *et al.* (2000) as:

$$\delta^{18}\text{O}_{\text{cell}}(\text{‰}) = p_{\text{ex}}(\delta^{18}\text{O}_{\text{XW}} + \varepsilon_{\text{wc}}) + (1 - p_{\text{ex}})(\delta^{18}\text{O}_{\text{NW}} + \varepsilon_{\text{wc}}) \quad \text{Eqn 6}$$

where p_{ex} is the proportion of exchangeable oxygen in cellulose formed, and ε_{wc} is the average fractionation between water and organic material. Since ε_{wc} depends on the temperature of the tissue where cellulose formation takes place, that is the cambium, we calculated it as described in Yakir and DeNiro (1990) and Sternberg and Ellsworth (2011):

$$\varepsilon_{\text{wc}} = 0.0084 T^2 - 0.51 T + 33.172 \quad \text{Eqn 7}$$

Also for this analysis, $\delta^{18}\text{O}$ data from needle and xylem water were time integrated by averaging values of the period when each tree-ring section was in the cell wall formation phase. As mentioned above, only periods with overlap between cell wall formation and available xylem and needle water measurements were considered for these analyses.

By using Eqn 6 and our observed $\delta^{18}\text{O}$ data of xylem and needle water and tree-ring cellulose, we then calculated p_{ex} along the growing season, for each site and study year (2012–2013). Generalized additive models were applied to smooth trends along the growing season and calculate confidence intervals. To test whether aridity or turnover of the sucrose pool available for cellulose synthesis has a major influence on p_{ex} , linear models were fitted to explain the obtained p_{ex} as a function of VPD and duration of cell wall formation (as a surrogate of carbohydrate demand) as explanatory variables. Model selection and reduction in explanatory variables were done based on Akaike’s information criteria (AIC; Akaike, 1974). We considered models with substantial support to be those with $\text{AIC} < 2$. Root mean square error (RMSE) and mean absolute error (MAE) were also quantified for all the models.

All statistical analyses were performed in the R environment v.4.1.2 (R Development Core Team, 2015) and graphics were designed using the R package GGPlot2 (Wickham, 2009).

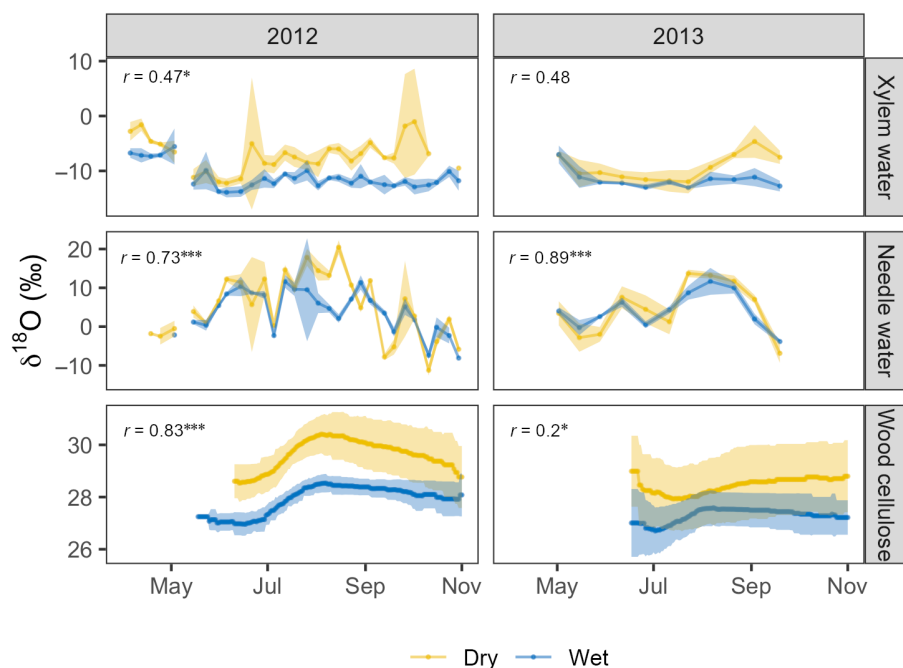


Fig. 2 Seasonal $\delta^{18}\text{O}$ variations of xylem and needle water and tree-ring cellulose. Colored ribbons correspond to \pm SD. Pearson correlation coefficients (r) between the series of both sites are also displayed. *, $P \leq 0.05$; ***, $P \leq 0.001$.

Results

Site conditions

While seasonal variations in VPD were similar at both sites, mean VPD was consistently slightly higher at the dry site, specifically in summer (Fig. 1c). Trees from the dry site, however, transpired significantly less than those from the wet site from mid-July to the end of September in 2012 and 2013 (Fig. 1d). The transpiration rates in 2013 were lower compared with the previous year at both sites. At the dry site, rocky soil conditions promoted drainage of the different soil layers, whereas at the wet site, the small perennial stream saturated the deep soil layers and maintained a high soil water content in the shallow layer (65%) during the two study years (Fig. 1e). At the dry site, the soil water content was lower at both layers (shallow 12% and deep 25%) and the year 2013 stands out as the year with the highest water supply in deep soil layers until the beginning of August and in the shallow layer until mid-June.

Patterns of $\delta^{18}\text{O}$ along tree compartments

The intra-annual mean levels of xylem water $\delta^{18}\text{O}$ differed between sites (Figs 2, S4, S5). In general, xylem water was significantly ^{18}O enriched at the dry site in comparison with the wet site ($P < 0.001$). Temporal, that is week-to-week variations, however, correlated significantly between sites only in 2012. In this year, mean xylem water $\delta^{18}\text{O}$ values decreased at the beginning of the growing season at both sites and then increased during the growing season at the dry site, whereas they remained relatively stable at the wet site. In 2013, however, mean xylem water $\delta^{18}\text{O}$ values were similar at both sites during the first part of the

growing season (until the beginning of August), but significantly differed after.

Mean needle water $\delta^{18}\text{O}$ values were overall not significantly different between sites. Needle water $\delta^{18}\text{O}$ values increased at both sites at the beginning of the growing season toward a maximum in August, and afterward steadily decreased toward the end of the growing season. Temporal (week-to-week) variations of needle water $\delta^{18}\text{O}$ values were significantly correlated between both sites ($r = 0.68$ – 0.89), except for a short period in August 2012.

Mean tree-ring cellulose $\delta^{18}\text{O}$ values were significantly higher at the dry site than at the wet site ($P < 0.001$) in 2012 but not in 2013. This difference was also observed regarding the temporal variations: tree-ring cellulose $\delta^{18}\text{O}$ values first increased at the beginning of the growing season, reaching their maximum in August 2012 (30.41‰ dry site and 28.53‰ wet site; Figs 2, S3). Afterward, values either remained relatively stable or decreased. In 2013, we observed a similar temporal pattern as in 2012 for the wet site, with a maximum of 27.58‰ reached in August. The tree-ring cellulose $\delta^{18}\text{O}$ pattern of the dry site in 2013, however, differed with low values in July and August, and relatively stable values afterward.

The intra-annual soil water $\delta^{18}\text{O}$ values (5 and 60 cm soil depth) remained relatively stable at the wet site while they partially increased toward summer at the dry site (Fig. S4).

Relations among pathway components

Substantial differences in the outcomes of the SEMs were observed between sites (Fig. 3; Table 1). At the wet site, the soil water $\delta^{18}\text{O}$ values of both depths were positively related and contributed equally to the xylem water $\delta^{18}\text{O}$ values. Needle water $\delta^{18}\text{O}$ values were strongly positively related to xylem water $\delta^{18}\text{O}$

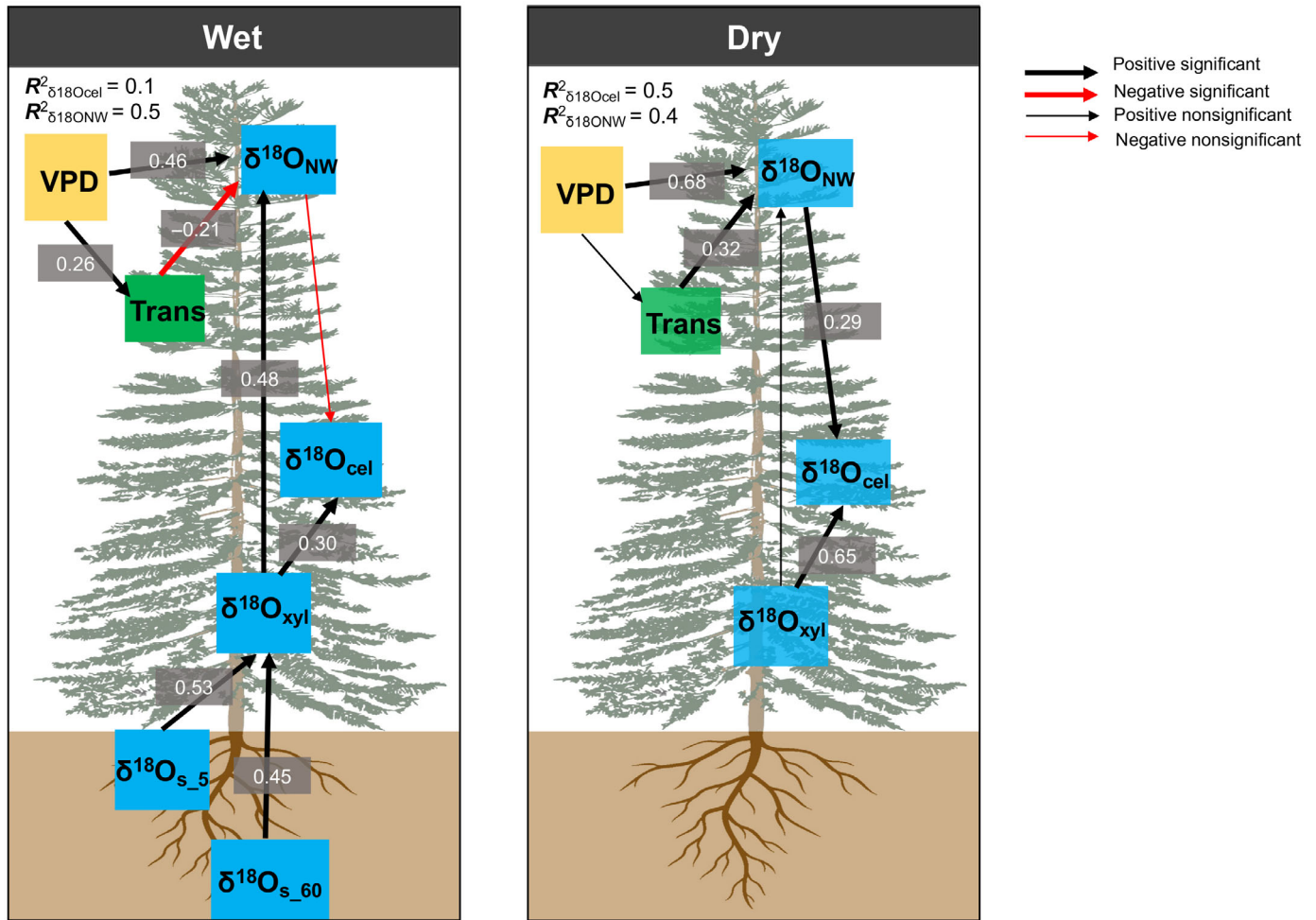


Fig. 3 Structural equation models assessing the changes in $\delta^{18}\text{O}$ along tree isotopic pathway for the two study sites. Standardized estimates of the regression coefficients are provided. Soil water could only be included at the wet site. CFI, comparative fit index; RMSEA, root mean square error of approximation; *Trans*, transpiration rates; VPD, vapor pressure deficit; $\delta^{18}\text{O}_{\text{cel}}$, $\delta^{18}\text{O}$ of tree-ring cellulose; $\delta^{18}\text{O}_{\text{NW}}$, $\delta^{18}\text{O}$ of needle water; $\delta^{18}\text{O}_{\text{s}_5}$, $\delta^{18}\text{O}$ of soil water at 5 cm depth; $\delta^{18}\text{O}_{\text{s}_60}$, $\delta^{18}\text{O}$ of soil water at 60 cm depth; $\delta^{18}\text{O}_{\text{XYL}}$, $\delta^{18}\text{O}$ of xylem water. CFI ranges from 0 to 1 with larger values indicate better fit.

values. Both needle water $\delta^{18}\text{O}$ values and the ^{18}O -enrichment above xylem water ($\Delta^{18}\text{O}$) were positively related to VPD and negatively to RH, respectively (Figs S6a,b, S7a,b). Transpiration was significantly positively related to VPD and significantly negatively related to needle water $\delta^{18}\text{O}$ values. However, needle water $\delta^{18}\text{O}$ values did not contribute significantly to the final tree-ring cellulose $\delta^{18}\text{O}$ values, whereas xylem water $\delta^{18}\text{O}$ values contributed significantly positively.

At the dry site, needle water $\delta^{18}\text{O}$ values were positively related to VPD and needle water (also ^{18}O -enrichment above xylem water, Fig. S6b). Xylem water $\delta^{18}\text{O}$ values did not significantly contribute to needle water $\delta^{18}\text{O}$ values, though a slightly positive effect was observed. In contrast to the wet site, transpiration had a positive effect on needle water $\delta^{18}\text{O}$ values. Both needle water and xylem water $\delta^{18}\text{O}$ values contributed significantly positively to tree-ring cellulose $\delta^{18}\text{O}$ values, but xylem water $\delta^{18}\text{O}$ had a stronger role.

Overall, SEMs showed lower CFI and higher RMSEA at the wet site (CFI = 0.50, RMSEA = 0.18) in comparison with

the dry site (CFI = 0.99, RMSEA = 0.01). The overall explained variance of needle water $\delta^{18}\text{O}$ was high at both sites (wet 0.5 and dry 0.4) but reduced for tree-ring cellulose $\delta^{18}\text{O}$ for the wet site (wet 0.1 and dry 0.4).

Both needle water and tree-ring cellulose $\delta^{18}\text{O}$ values could be explained by VPD and RH variations (Figs S6, S7). The significant relation between tree-ring cellulose $\delta^{18}\text{O}$ values and VPD (or RH) did not remain when assessing the relation of VPD (and RH) with the enrichment of tree-ring cellulose $\delta^{18}\text{O}$ values over source water ($\Delta^{18}\text{O}$; Figs S6, S7c,d). The relation between observed needle water and tree-ring cellulose enrichments was not significant for most of the study years and sites (Fig. S8).

Performance of mechanistic needle water models

The C–G model and the Péclet modification both overall showed good predictive skills for the $\delta^{18}\text{O}$ values of needle water (Figs 4, S9) and enrichment (Fig. S10), with a positive slope of the regression line close to 1 : 1. The C–G model explained 40%

Table 1 Parameters defining the structural equation model (SEM) with standardized estimate coefficients, the standardized estimate coefficient error, z-value, and *P*-value for both sites.

Site	Regression	Regressor	Estimate	SE	z-Value	<i>P</i> (> z)
Wet	$\delta^{18}\text{O}_{\text{XYL}}$	$\delta^{18}\text{O}_{\text{s}_5}$	0.53	0.072	7.28	< 0.001
		$\delta^{18}\text{O}_{\text{s}_60}$	0.45	0.072	6.17	< 0.001
	$\delta^{18}\text{O}_{\text{NW}}$	$\delta^{18}\text{O}_{\text{XYL}}$	0.48	0.083	5.72	< 0.001
		Trans	-0.21	0.119	-1.74	0.081
	VPD	VPD	0.46	0.065	7.10	< 0.001
		VPD	0.26	0.113	1.39	< 0.001
$\delta^{18}\text{O}_{\text{cell}}$	$\delta^{18}\text{O}_{\text{NW}}$	-0.17	0.126	-1.32	0.163	
	$\delta^{18}\text{O}_{\text{XYL}}$	0.30	0.114	2.63	0.009	
Dry	$\delta^{18}\text{O}_{\text{NW}}$	$\delta^{18}\text{O}_{\text{XYL}}$	0.29	0.116	2.52	0.012
		Trans	0.32	0.073	4.49	< 0.001
	VPD	VPD	0.68	0.075	9.12	< 0.001
		VPD	0.10	0.103	1.12	0.215
	$\delta^{18}\text{O}_{\text{cell}}$	$\delta^{18}\text{O}_{\text{NW}}$	0.29	0.085	3.47	< 0.001
		$\delta^{18}\text{O}_{\text{XYL}}$	0.65	0.059	11.09	< 0.001

Trans, transpiration rates; VPD, vapor pressure deficit; $\delta^{18}\text{O}_{\text{cell}}$, $\delta^{18}\text{O}$ of tree-ring cellulose; $\delta^{18}\text{O}_{\text{NW}}$, $\delta^{18}\text{O}$ of needle water; $\delta^{18}\text{O}_{\text{s}_5}$, $\delta^{18}\text{O}$ of soil water at 5 cm depth; $\delta^{18}\text{O}_{\text{s}_60}$, $\delta^{18}\text{O}$ of soil water at 60 cm depth; $\delta^{18}\text{O}_{\text{XYL}}$, $\delta^{18}\text{O}$ of xylem water.

and 57% of the variance for the wet and dry site, respectively. The Pécelet modification explained slightly more of the variance than the C–G model for the dry site but the same variance as the C–G model at the wet site. Furthermore, the RMSE of the Pécelet modification was lower for the dry site compared with the C–G model but not for the wet site, suggesting a better fit of the predictions only at the dry site. The analyses of the fractional difference between predicted and observed bulk needle water enrichment at the evaporation sites (*f*) suggested that both the C–G model and the Pécelet modification overestimated the needle enrichment at the dry site (Fig. S11). At the wet site, the C–G model slightly overestimated the needle enrichment (0.06) whereas the Pécelet modification underestimated it (−0.13). The

yearly based outcome of the models did not differ from the main patterns (Figs S9, S10).

Seasonal variations in p_{ex} and its relation to VPD

Importantly, p_{ex} showed strong variations along the position of the ring as well as along the growing season and was different between sites and years (Fig. 5). In 2012, p_{ex} values significantly differed between sites for a large percentage of the ring (Fig. 5a). At the dry site, p_{ex} continuously increased and reached on average, a maximum of 0.50 at 55% of the ring. At the wet site, p_{ex} remained stable for the first 50% of the ring and then steadily decreased. In 2013, however, both sites displayed similar p_{ex} values for the first half of the ring but differed afterward. The initial p_{ex} values were lower in comparison with the previous year (0.38 and 0.15). They increased to 0.38 at the wet site (60% of the ring) and even more increased at the dry site toward a maximum of 0.52 at 75% of the ring. We could not calculate p_{ex} variations during the last 13% of the 2013 ring due to missing needle and xylem water $\delta^{18}\text{O}$ measurements at the end of cell wall formation (November; Fig. 5). We also observed a notable level of variability in the p_{ex} levels among trees, particularly at the wet site during the year 2012.

The intra-annual analyses of the p_{ex} values revealed the uneven relationships between the intra-ring position and the timing of ring formation (Fig. 5b). Maximum levels of p_{ex} were reached, in general, in the summer (late July and the beginning of August). In 2012, p_{ex} was significantly higher at the dry site than at the wet site from the beginning of the growing season until October, and consistently above the maximum of the wet site from June to September. In 2013, p_{ex} values were similar at both sites during a 1-month period (from mid-June to mid-July). From mid-July to mid-September, the p_{ex} values were significantly higher at the dry site than at the wet site. We could not calculate p_{ex} for the last part of the 2013 growing season.

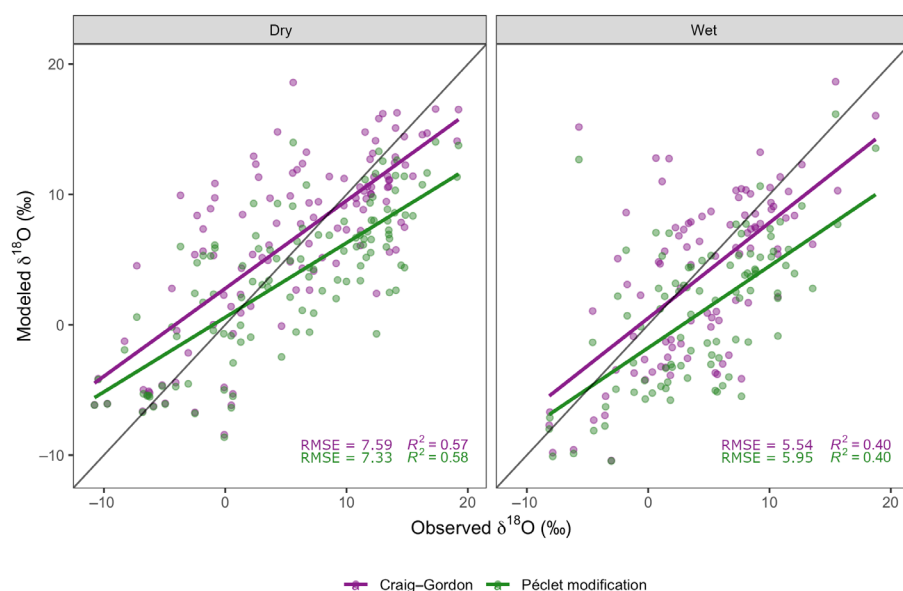


Fig. 4 Mechanistic modeling of the needle water enrichment above the source water (Δ) for both study sites and years. The Craig–Gordon model and the Pécelet modification were applied. See Supporting Information Notes S2 for the description of the parameters. Solid lines represent the 1 : 1 relationship.

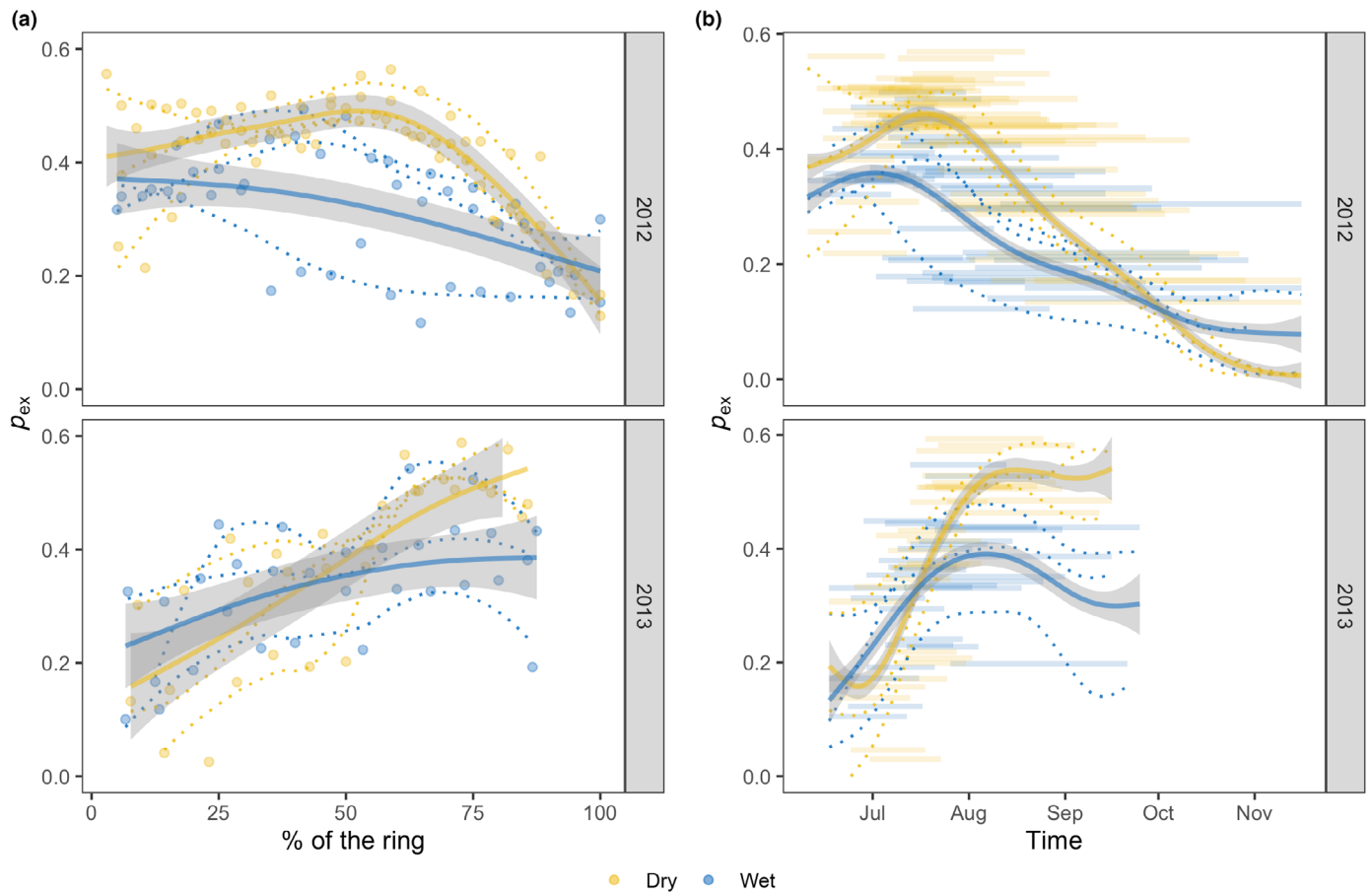


Fig. 5 Intra-annual changes in p_{ex} for the two study years and sites aligned by ring position (a) and time of cell wall formation (b). Dotted lines indicate individual tree measurements. Horizontal lines in b represent individual periods of cell wall formation of the 50- μ m intra-annual sectors. The main trends were highlighted using a GAM function, with shading representing the 95% confidence interval.

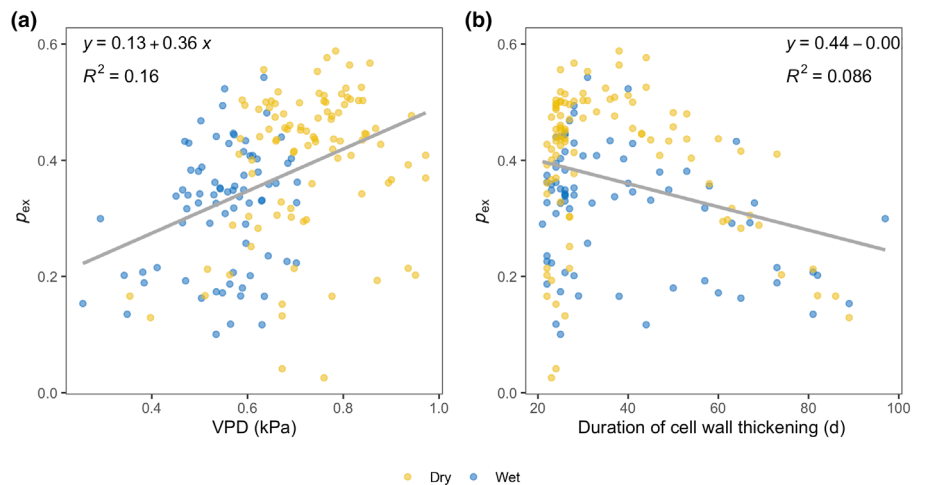


Fig. 6 Relation between the proportion of oxygen atom exchange (p_{ex}) and vapor pressure deficit (VPD) at the time of cell wall formation (a), and the duration of cell wall formation (b). Related statistics are shown in Table 2.

The results of the linear models highlighted VPD as a slightly better driver of p_{ex} variations than the time of cell wall formation (Fig. 6; Table 2). This was deduced based on the AIC of the linear models, with the lowest AIC values obtained in those models with VPD as the main predictor. The variance explained by the selected model was 16%, with a positive relation between p_{ex} and

VPD. Similar explained variance (14%) could be assessed with RH as a predictor (Fig. S12). By contrast, the model that has the time of cell wall formation as the main predictor showed higher AIC scores and explained a lower percentage of variance (9%). RMSE and MAE values were also slightly better for the models using VPD as a predictor. A third model accounting for the

Table 2 Summary of the comparison among linear models to explain the proportion of oxygen exchange (p_{ex}).

	AIC	R^2 (%)	RMSE	MAE
$p_{ex} \sim$ Vapor pressure deficit	-240.24	16.48***	0.12	0.09
$p_{ex} \sim$ Time of cell wall formation	-216.55	8.57***	0.11	0.10
$p_{ex} \sim$ Vapor pressure deficit \times Time of cell wall formation	-238.25	15.10***	0.11	0.10

AIC, Akaike's information criteria; MAE, mean absolute error; RMSE, root mean square error.

*** $P \leq 0.001$.

interaction between both predictors was also assessed. Although explaining a similar portion of variance compared with the simple model with VPD, it scored higher AIC values, and the time of cell wall formation had no significant effect.

Discussion

We have quantified the relative contribution of all the elements of the pathway that influence the final $\delta^{18}\text{O}$ signatures of tree-ring cellulose of larch trees growing in the Swiss Alps. Atmospheric evaporative demand is the major control of needle water enrichment whereas transpiration has the opposite effect at the two sites due to differential stomatal activity. This opposite effect could be an indirect sign of the Péclet effect since higher transpiration leads to more back-forward diffusion of water in the needles. The differential effect of transpiration between sites, however, was not captured by the mechanistic models when accounting for the Péclet effect. Our results indicate a stronger relationship between stem cellulose and xylem water than needle water at both sites. This fact can be explained by the rate of oxygen atom exchange between sugars and source water during cellulose synthesis. By including information about cell wall formation derived from xylogenesis, we observed that maximum p_{ex} values were achieved in August and imprinted sections located toward the last part of the ring (50–75%). Furthermore, high p_{ex} values were better associated with periods of high atmospheric evaporative demand than with the time of cell formation during the growing season.

Water $\delta^{18}\text{O}$: soil, xylem, and needles

Xylem water $\delta^{18}\text{O}$ directly mirrored the differences in soil water $\delta^{18}\text{O}$ between sites with lower and less variable values at the wet site. In general, root water uptake has been determined as a non-fractionation process (Dawson & Ehleringer, 1991). Therefore, these differences can be potentially explained by groundwater conditions and the mixing of water pools at the wet site vs a dominant effect of actual precipitation at the dry site. Needle water at both sites did generally not differ in terms of seasonal distribution and variability indicating a strong common driver. Indeed, the results of our SEMs clearly demonstrate a close relation to evaporative atmospheric demand. In line with ours, recent studies have highlighted the strong relationship between leaf water $\delta^{18}\text{O}$ with relative air humidity, which is highly correlated

to VPD (Cernusak *et al.*, 2022). Interestingly, the effect of transpiration on needle water $\delta^{18}\text{O}$ was, however, opposite at both sites according to our SEMs. A positive relationship between transpiration and needle water $\delta^{18}\text{O}$ values at the dry site relates to the fact that transpiration is strongly curtailed to avoid water losses under reduced soil water availability, and under low transpiration leaf water ^{18}O enrichment is mainly dominated by atmospheric demand. At the wet site, transpiration seems to be less restricted. During the period of highest transpiration (July 2012), we observed, however, lower leaf water enrichment compared with the dry site. This, together with a negative relationship between transpiration and needle water $\delta^{18}\text{O}$ in the SEMs, could be a potential indicator of the Péclet effect (Farquhar & Lloyd, 1993). In this case, high transpiration rates could induce a high advection of nonenriched xylem water as opposed to back-diffusion of enriched water from the sites of evaporation resulting in less enriched needle water.

The Péclet effect is still seen quite controversial since it should not be taken for granted in all species (Barbour *et al.*, 2021) and its parametrization requires a comprehensive characterization (Kahmen *et al.*, 2009). The output of the mechanistic models, however, did not provide clear evidence of the Péclet effect. Indeed, modeled needle water $\delta^{18}\text{O}$ did not substantially differ when using the C–G model or the Péclet modification. When assessing modeled $\Delta^{18}\text{O}$ and f , these were overestimated at the dry site by both models; whereas at the wet site, they were either overestimated or underestimated according to the C–G or the Péclet modification, respectively. Our extended observational data and modeling outcome support initial findings from few empiric studies on the Péclet effect and that it is not constant over the growing season (Song *et al.*, 2013), and has a minor impact on needle water enrichment of conifers (Barbour *et al.*, 2021; Lin *et al.*, 2022). However, accurate atmospheric water vapor $\delta^{18}\text{O}$ measurements may improve modeling results and help in further highlighting differences in needle water enrichment.

Cellulose $\delta^{18}\text{O}$ signatures and their links to xylem water, needle water, and VPD

The SEMs revealed that xylem water $\delta^{18}\text{O}$ plays a major role in determining the tree-ring $\delta^{18}\text{O}$ levels. The contribution of xylem water $\delta^{18}\text{O}$ can be also observed when comparing sites. Despite showing almost no differences in needle water dynamics, tree-ring $\delta^{18}\text{O}$ values differed significantly as also observed in xylem water $\delta^{18}\text{O}$ values. This strong signal of the source water signature is actually the basis for other studies that demonstrated that precipitation $\delta^{18}\text{O}$ has a strong influence on tree-ring $\delta^{18}\text{O}$ series and serves, for instance, to capture tropical cyclone activity (Miller *et al.*, 2006; Altman *et al.*, 2021). Indeed, Offermann *et al.* (2011) reported that $\delta^{18}\text{O}$ in the phloem organic matter correlated better with the $\delta^{18}\text{O}$ in soil and xylem water than with leaf water evaporative enrichment, suggesting a seasonally varying contribution of different carbohydrate sources to tree-ring formation.

When assessing the intra-annual patterns, we observed a general increase in intra-annual cellulose $\delta^{18}\text{O}$ values during the

beginning of the growing season toward a maximum enrichment in July–August, and a depletion after. This pattern resembles the seasonal patterns of needle water dynamics, however, with reduced high-frequency fluctuations compared with the latter. This also suggests a subtle imprint of needle water $\delta^{18}\text{O}$ (and VPD as its climatic driver) on the dynamics of intra-annual tree-ring cellulose $\delta^{18}\text{O}$. Indeed, a positive relation between intra-annual tree-ring cellulose $\delta^{18}\text{O}$ values and VPD (and RH) was observed at our study sites, although weaker than the needle water $\delta^{18}\text{O}$ –VPD relationship. This link between tree-ring $\delta^{18}\text{O}$ values and atmospheric water demand has been previously reported at inter-annual (Vitali *et al.*, 2021) and also at intra-annual resolution (Belmecheri *et al.*, 2018; Szejner *et al.*, 2020; Xu *et al.*, 2022). However, the VPD signal of intra-annual tree-ring cellulose $\delta^{18}\text{O}$ values disappears when expressing cellulose $\delta^{18}\text{O}$ as isotopic enrichment above xylem water ($\Delta^{18}\text{O}$). The cellulose enrichment above xylem water does not significantly relate to the observed enrichment of needle water above xylem water, potentially indicating that the VPD signal is recorded during processes related to both source water and needle water enrichment.

p_{ex} is highly variable along the growing season and related to VPD

This major contribution of xylem water to the intra-annual cellulose $\delta^{18}\text{O}$ signature can be explained by changes in the proportion of oxygen atom exchange with unenriched xylem water. Among all the isotope fractionation steps along the oxygen isotope pathway from the soil water to the tree ring, p_{ex} still remains one of the least understood (Song *et al.*, 2022). Our results suggest that p_{ex} needs to be variable in order to accurately predict the observed intra-annual tree-ring cellulose $\delta^{18}\text{O}$ variations. A wide range of literature assumed a constant value of p_{ex} *c.* 0.42 (Roden *et al.*, 2000; Cernusak *et al.*, 2005), but our study is in line with those suggesting a nonconstant p_{ex} which can vary between sites and environmental conditions (Gessler *et al.*, 2009) as well as throughout the growing season (Offermann *et al.*, 2011; Xu *et al.*, 2022). In comparison with our results, however, Offermann *et al.* (2011) found a decrease in p_{ex} from spring to mid-summer in phloem organic matter, which is in contradiction with our observed seasonal patterns. We also noted a certain degree of variation in the individual p_{ex} measurements among the trees, which could potentially be mitigated by including a larger number of individuals in the study.

Some studies assign p_{ex} variations to turnover rates of the non-structural carbohydrates indirectly controlled by source–sink dynamics (Song *et al.*, 2014; Gessler & Treydte, 2016). Following this assumption, we initially expected that long periods of cell wall formation, either due to the common patterns (early- vs late-wood) and/or triggered by environmental constraints (e.g. drought; see Cuny *et al.*, 2014), would imply slow tree metabolism, low sink demand and, potentially, high exchange with unenriched water via triose-phosphate cycling. Our results indicate, however, that the duration of cell wall formation did not satisfactorily explain the observed variations of p_{ex} along the growing season since earlywood sections of the tree rings

displayed similar p_{ex} values as latewood ones, despite contrasting cell formation dynamics (earlywood: fast cell development, high sink demand; latewood: slow cell development, low sink demand). We rather found that a dry atmosphere (high VPD) was a good predictor for intra-annual changes in p_{ex} and differences between sites. Although significant, the variance of p_{ex} explained by VPD was relatively low ($r^2 = 0.16$). However, it is important to consider that VPD was integrated over time, taking into account the cell formation period for each cut, and this time integration may have dampened the signal. Cheesman and Cernusak (2016) found that p_{ex} was strongly coupled to relative humidity when analyzing branch cellulose from 11 sites across Australia. The observed difference in p_{ex} between the dry and wet sites in our study seems consistent with these results. Our study even goes beyond by also finding this relationship at a higher resolved temporal scale (intra-annual). p_{ex} and its drivers have been mainly studied at leaf level, and there, the relation between p_{ex} and relative humidity or VPD (Lehmann *et al.*, 2017; Hirl *et al.*, 2021) is usually opposite (higher p_{ex} with high RH or low VPD) compared with our study. The isotope effects during phloem loading, unloading and transport, and/or the different climatic drivers of leaf and wood cellulose may be relevant to explain such inconsistencies. Besides, potential water storage effects in the phloem and species-specific dynamics in radial water movement between inner bark and sapwood may also play a role (Treydte *et al.*, 2021), but have been rarely studied in adult trees up to now.

Other studies found an indirect relation between intra-annual changes in p_{ex} and cell anatomical characteristics in *Pinus ponderosa* (Szejner *et al.*, 2020). The authors suggest that earlywood cells (with larger lumen areas) were under a lower oxygen atom exchange than those cells with smaller lumen areas from the latewood section, partly explained by both changes in aridity and turnover rates. Our findings support the relation between aridity and p_{ex} also observed in the results from Szejner *et al.* (2020) but do not sustain the relation with the turnover rates. We did not observe the highest p_{ex} values in the latewood sections of the rings (those with the smallest lumen area in a typical conifer-type tree ring), but rather in those sections that did form during the highest atmospheric moisture demand. Those sections were located *c.* 50–75% of the ring, which are not usually the sections with the smallest cell lumen areas in a typical conifer (Fritts *et al.*, 1991). Even some latewood sections carried lower p_{ex} values than some earlywood sections. Indeed, cell lumen areas in conifers are the result of the combination of two distinct processes with independent environmental cues, that is cell enlargement and wall thickening (Cuny *et al.*, 2014). This fact complicates the interpretation of the link between lumen area, environmental drivers, and their stable isotopic composition. Although we did not analyze wood anatomical measurements, our xylogenesis data allowed to disentangle both processes. Specifically, the timing of cell wall development is the best parameter to assign intra-annual stable isotopic signatures to a specific time and to benchmark mechanistic models (see also Belmecheri *et al.*, 2018; Martínez-Sancho *et al.*, 2022). However, the last latewood sections need to be carefully interpreted since they grow over long periods

(months) and therefore integrate a larger range of environmental conditions. A more adaptive size of the sections according to cell ontogeny could help to solve this challenge (e.g. smaller sections; < 50 μm in the latewood part). Furthermore, movement of carbohydrates into and out of reserve pools (e.g. starch) could also complicate the situation (Gessler *et al.*, 2007), further altering the calculated p_{ex} . Increasing the number of studied individuals might be helpful to find stronger patterns.

Implications for tree-ring $\delta^{18}\text{O}$ studies

The debate about which physiological mechanisms govern $\delta^{18}\text{O}$ variations in tree-ring series is currently very intense and controversial (see the Discussion section; Guerrieri *et al.*, 2022; Lin *et al.*, 2022). Since $\delta^{18}\text{O}$ is not affected by fractionation due to photosynthetic assimilation, its combination with $\delta^{13}\text{C}$ has been proposed as a suitable technique to distinguish whether a change in isotope ratios is the result of a change in photosynthesis rate or stomatal conductance (i.e. dual-isotope approach, Scheidegger *et al.*, 2000; Grams *et al.*, 2007). The center of the discussion focuses on how faithfully $\delta^{18}\text{O}$ variations in tree rings represent the dynamics of leaf water enrichment driven by VPD (and thus linked to stomatal conductance) and transpiration. Indeed, the $g_s-\Delta^{18}\text{O}$ relation is more complex and variable than previously hypothesized with still some caveats such as the role of the Péclet effect. More importantly, these conceptual models were developed for the leaf level, and the oxygen exchange during cellulose synthesis in the stem cambium is mostly ignored.

Here, we provide, for the first time, a mechanistically in-depth understanding of the key fractionation and oxygen atom exchange processes involved in the overall tree-ring $\delta^{18}\text{O}$ signature. This goes beyond previous studies that associated variations of the cellulose $\delta^{18}\text{O}$ signature mainly with variations in source water $\delta^{18}\text{O}$ values (Treydte *et al.*, 2014). We demonstrate that although the intra-annual seasonal variations mirrored to some degree seasonal variations of needle water $\delta^{18}\text{O}$ variability and are linked to VPD variations, the mean annual tree-ring cellulose $\delta^{18}\text{O}$ values were, however, strongly influenced by the xylem water $\delta^{18}\text{O}$ signatures. This fact is crucial for the tree-ring community since most of the studies using tree-ring $\delta^{18}\text{O}$ series analyze the year-to-year variability (one sample per ring, average annual level), which may include reduced information derived from leaf-level processes based on our results. The specific characteristic of our framework highlights that xylem water $\delta^{18}\text{O}$ is mainly dominated by soil water content and its isotopic signature. Evaporative drivers in soil processes may leave a relevant imprint in source water and therefore get recorded in tree-ring $\delta^{18}\text{O}$.

Early in the 80s, Burk and Stuiver (1981) already suggested that covariation between air dryness and soil dryness could mask $\delta^{18}\text{O}$ cellulose signals. Both, to some degree, can covariate due to common climatic drivers (e.g. VPD) but the thresholds and fractionation mechanisms that occur in each compartment are specific. In line with this statement, we claim that most of the climatic signals encoded in inter- and intra-annual tree-ring cellulose $\delta^{18}\text{O}$ series could come from climatic drivers of fractionation

processes affecting source water rather than leaf water. Better understanding fractionation steps and climatic drivers related to the spatial variation of the precipitation $\delta^{18}\text{O}$ signature (Nelson *et al.*, 2021), mixing of water pools and root uptake (Gessler *et al.*, 2022), the potential uncoupling of soil water and xylem pools (Barbeta *et al.*, 2020) and/or water exchange during loading of sugars in phloem transport (Offermann *et al.*, 2011) are necessary points of the research agenda to disentangle the origin of the climatic signals in intra- and inter-annual tree-ring $\delta^{18}\text{O}$ series.

Acknowledgements

We thank Daniel Pock, Lara Widmer, and Leandra Méndez Tobler for helping pack samples; Loic Schneider, Manuela Oetti, Daniel Nievergelt, and Holger Gärtner for support with laboratory logistics; and Esteban Guevara for advice with the structural equation models. This study was funded by the Swiss National Science Foundation through projects TROXY (grant no. 175888; KT and EM-S), ISOPATH (grant no. 200021_130112; KT), LOTFOR (grant no. 150205; PF), and TreeCarbo (grant no. 179978; MML).




Competing interests

None declared.

Author contributions

KT and EM-S designed the study. AGr prepared and performed the sections for intra-annual isotope measurements. PF contributed with transpiration and wood formation data. BU prepared the soil, xylem, and needle water data. EGP installed and contributed to the soil water measurements. MS performed the tree-ring isotopic measurements. EM-S performed the statistical analyses and the mechanistic modeling with help from LAC and AGE. EM-S led the writing of the manuscript. All authors (EM-S, LAC, PF, AGr, BU, EGP, AGE, MML, MS and KT) contributed to the final version of the manuscript.

ORCID

Lucas A. Cernusak  <https://orcid.org/0000-0002-7575-5526>
 Patrick Fonti  <https://orcid.org/0000-0002-7070-3292>
 Arthur Gessler  <https://orcid.org/0000-0002-1910-9589>
 Marco M. Lehmann  <https://orcid.org/0000-0003-2962-3351>
 Elisabet Martínez-Sancho  <https://orcid.org/0000-0003-4413-6818>
 Elisabeth Graf Pannatier  <https://orcid.org/0000-0003-2676-2583>
 Matthias Saurer  <https://orcid.org/0000-0002-3954-3534>
 Kerstin Treydte  <https://orcid.org/0000-0001-8399-6517>

Data availability

The datasets analyzed in this study are available in doi: <https://doi.org/10.16904/envidat.432>.

References

- Akaike H. 1974. A new look at statistical model identification. *IEEE Transactions on Automatic Control* 19: 716–722.
- Altman J, Saurer M, Dolezal J, Marekova N, Song J-S, Ho C-H, Treydte K. 2021. Large volcanic eruptions reduce landfalling tropical cyclone activity: evidence from tree rings. *Science of the Total Environment* 775: 145899.
- Arx GV, Carrer M. 2014. ROXAS – a new tool to build centuries-long tracheid-lumen chronologies in conifers. *Dendrochronologia* 32: 290–293.
- Barbata A, Gimeno TE, Clavé L, Fréjaville B, Jones SP, Delvigne C, Wingate L, Ogée J. 2020. An explanation for the isotopic offset between soil and stem water in a temperate tree species. *New Phytologist* 227: 766–779.
- Barbour MM, Farquhar GD. 2000. Relative humidity- and ABA-induced variation in carbon and oxygen isotope ratios of cotton leaves. *Plant, Cell & Environment* 23: 473–485.
- Barbour MM, Loucos KE, Lockhart EL, Shrestha A, McCallum D, Simonin KA, Song X, Griffani DS, Farquhar GD. 2021. Can hydraulic design explain patterns of leaf water isotopic enrichment in C₃ plants? *Plant, Cell & Environment* 44: 432–444.
- Belmecheri S, Wright WE, Szejner P, Morino KA, Monson RK. 2018. Carbon and oxygen isotope fractionations in tree rings reveal interactions between cambial phenology and seasonal climate. *Plant, Cell & Environment* 41: 2758–2772.
- Boettger T, Haupt M, Knöller K, Weise SM, Waterhouse JS, Rinne KT, Loader NJ, Sonninen E, Jungner H, Masson-Delmotte V *et al.* 2007. Wood cellulose preparation methods and mass spectrometric analyses of $\delta^{13}\text{C}$, $\delta^{18}\text{O}$, and nonexchangeable $\delta^2\text{H}$ values in cellulose, sugar, and starch: an interlaboratory comparison. *Analytical Chemistry* 79: 4603–4612.
- Büntgen U, Urban O, Krusic PJ, Rybníček M, Kolář T, Kyncl T, Ač A, Koňasová E, Čáslavský J, Esper J *et al.* 2021. Recent European drought extremes beyond Common Era background variability. *Nature Geoscience* 14: 190–196.
- Burk RL, Stuiver M. 1981. Oxygen isotope ratios in trees reflect mean annual temperature and humidity. *Science* 211: 1417–1419.
- Cernusak LA, Barbata A, Bush RT, Eichstaedt R, Ferrio JP, Flanagan LB, Gessler A, Martín-Gómez P, Hirl RT, Kahmen A *et al.* 2022. Do ^2H and ^{18}O in leaf water reflect environmental drivers differently? *New Phytologist* 235: 41–51.
- Cernusak LA, Barbour MM, Arndt SK, Cheesman AW, English NB, Feild TS, Helliker BR, Holloway-Phillips MM, Holtum JAM, Kahmen A *et al.* 2016. Stable isotopes in leaf water of terrestrial plants: stable isotopes in leaf water. *Plant, Cell & Environment* 39: 1087–1102.
- Cernusak LA, Farquhar GD, Pate JS. 2005. Environmental and physiological controls over oxygen and carbon isotope composition of Tasmanian blue gum, *Eucalyptus globulus*. *Tree Physiology* 25: 129–146.
- Cheesman AW, Cernusak LA. 2016. Infidelity in the outback: climate signal recorded in $\Delta^{18}\text{O}$ of leaf but not branch cellulose of eucalypts across an Australian aridity gradient. *Tree Physiology* 37: 554–564.
- Craig H, Gordon LI. 1965. Deuterium and oxygen-18 variations in the ocean and the marine atmosphere. In: *Proceedings of a conference on stable isotopes in oceanographic studies and palaeotemperatures*. Lischi and Figli, Pisa, 9–130.
- Cuny HE, Fonti P, Rathgeber CBK, Arx GV, Peters RL, Frank DC. 2019. Couplings in cell differentiation kinetics mitigate air temperature influence on conifer wood anatomy. *Plant, Cell & Environment* 42: 1222–1232.
- Cuny HE, Rathgeber CBK, Frank D, Fonti P, Fournier M. 2014. Kinetics of tracheid development explain conifer tree-ring structure. *New Phytologist* 203: 1231–1241.
- Cuny HE, Rathgeber CBK, Frank D, Fonti P, Makinen H, Prislán P, Rossi S, Del Castillo EM, Campelo F, Vavřík H *et al.* 2015. Woody biomass production lags stem-girth increase by over one month in coniferous forests. *Nature Plants* 1: 1–6.
- Cuny HE, Rathgeber CBK, Kiessé TS, Hartmann FP, Barbeito I, Fournier M. 2013. Generalized additive models reveal the intrinsic complexity of wood formation dynamics. *Journal of Experimental Botany* 64: 1983–1994.
- Dawson TE, Ehleringer JR. 1991. Streamside trees that do not use stream water. *Nature* 350: 335–337.
- Deslauriers A, Beaulieu M, Balducci L, Giovannelli A, Gagnon MJ, Rossi S. 2014. Impact of warming and drought on carbon balance related to wood formation in black spruce. *Annals of Botany* 114: 335–345.
- Ehleringer JR, Roden J, Dawson TE. 2000. Assessing ecosystem-level water relations through stable isotope ratio analyses. In: Sala OE, Jackson RB, Mooney HA, Howarth RW, eds. *Methods in ecosystem science*. New York, NY, USA: Springer, 181–198.
- Farquhar GD, Lloyd J. 1993. Carbon and oxygen isotope effects in the exchange of carbon dioxide between terrestrial plants and the atmosphere. In: *Stable isotopes and plant carbon-water relations*. Amsterdam, the Netherlands: Elsevier, 47–70.
- Ferrio JP, Cuntz M, Offermann C, Siegwolf R, Saurer M, Gessler A. 2009. Effect of water availability on leaf water isotopic enrichment in beech seedlings shows limitations of current fractionation models. *Plant, Cell & Environment* 32: 1285–1296.
- Foerstel H, Huetzen H. 1983. $^{18}\text{O}/^{16}\text{O}$ ratio of water in a local ecosystem as a basis of climate record. Vienna, Austria: International Atomic Energy Agency (IAEA).
- Fritts H, Vaganov E, Sviderskaya I, Shashkion A. 1991. Climatic variation and tree-ring structure in conifers: empirical and mechanistic models of tree-ring width, number of cells, cell size, cell-wall thickness and wood density. *Climate Research* 1: 97–116.
- Gessler A, Bächli L, Rouholahnejad Freund E, Treydte K, Schaub M, Haeni M, Weiler M, Seeger S, Marshall J, Hug C *et al.* 2022. Drought reduces water uptake in beech from the drying topsoil, but no compensatory uptake occurs from deeper soil layers. *New Phytologist* 233: 194–206.
- Gessler A, Brandes E, Buchmann N, Helle G, Rennenberg H, Barnard RL. 2009. Tracing carbon and oxygen isotope signals from newly assimilated sugars in the leaves to the tree-ring archive. *Plant, Cell & Environment* 32: 780–795.
- Gessler A, Ferrio JP, Hommel R, Treydte K, Werner RA, Monson RK. 2014. Stable isotopes in tree rings: towards a mechanistic understanding of isotope fractionation and mixing processes from the leaves to the wood. *Tree Physiology* 34: 796–818.
- Gessler A, Peuke AD, Keitel C, Farquhar GD. 2007. Oxygen isotope enrichment of organic matter in *Ricinus communis* during the diel course and as affected by assimilate transport. *New Phytologist* 174: 600–613.
- Gessler A, Treydte K. 2016. The fate and age of carbon – insights into the storage and remobilization dynamics in trees. *New Phytologist* 209: 1338–1340.
- Grams TEE, Kozovits AR, Häberle KH, Matussek R, Dawson TE. 2007. Combining $\delta^{13}\text{C}$ and $\delta^{18}\text{O}$ analyses to unravel competition, CO₂ and O₃ effects on the physiological performance of different-aged trees. *Plant, Cell & Environment* 30: 1023–1034.
- Guerrieri R, Belmecheri S, Asbjørnsen H, Xiao J, Hollinger DY, Clark K, Jennings K, Kolb TE, Munger JW, Richardson AD *et al.* 2022. Detecting long-term changes in stomatal conductance: challenges and opportunities of tree-ring $\delta^{18}\text{O}$ proxy. *New Phytologist* 236: 809–812.
- Hartl-Meier C, Zang C, Büntgen U, Esper J, Rothe A, Göttlén A, Dirnböck T, Treydte K. 2014. Uniform climate sensitivity in tree-ring stable isotopes across species and sites in a mid-latitude temperate forest. *Tree Physiology* 35: 4–15.
- Hill SA, Waterhouse JS, Field EM, Switsur VR, Ap RT. 1995. Rapid recycling of triose phosphates in oak stem tissue. *Plant, Cell & Environment* 18: 931–936.
- Hirl RT, Ogée J, Ostler U, Schäufele R, Baca Cabrera JC, Zhu J, Schleip I, Wingate L, Schnyder H. 2021. Temperature-sensitive biochemical ^{18}O -fractionation and humidity-dependent attenuation factor are needed to predict $\delta^{18}\text{O}$ of cellulose from leaf water in a grassland ecosystem. *New Phytologist* 229: 3156–3171.
- Hooper D, Coughlan J, Mullen M. 2008. Structural equation modelling: guidelines for determining model fit. *Electronic Journal of Business Research Methods* 6: 53–60.
- Kahmen A, Simonin K, Tu K, Goldsmith GR, Dawson TE. 2009. The influence of species and growing conditions on the ^{18}O enrichment of leaf water and its impact on ‘effective path length’. *New Phytologist* 184: 619–630.
- Labuhn I, Daux V, Girardclos O, Stievenard M, Pierre M, Masson-Delmotte V. 2016. French summer droughts since 1326 CE: a reconstruction based on tree ring cellulose $\delta^{18}\text{O}$. *Climate of the Past* 12: 1101–1117.
- Laumer W, Andreu L, Helle G, Schleser GH, Wieloch T, Wissel H. 2009. A novel approach for the homogenization of cellulose to use micro-amounts for

- stable isotope analyses. *Rapid Communications in Mass Spectrometry* 23: 1934–1940.
- Lehmann MM, Gamarra B, Kahmen A, Siegwolf RTW, Saurer M. 2017. Oxygen isotope fractionations across individual leaf carbohydrates in grass and tree species: $\delta^{18}\text{O}$ of individual leaf carbohydrates. *Plant, Cell & Environment* 40: 1658–1670.
- Lin W, Barbour MM, Song X. 2022. Do changes in tree-ring $\delta^{18}\text{O}$ indicate changes in stomatal conductance? *New Phytologist* 236: 803–808.
- Loader NJ, Young GHF, McCarroll D, Davies D, Miles D, Bronk RC. 2020. Summer precipitation for the England and Wales region, 1201–2000 CE, from stable oxygen isotopes in oak tree rings. *Journal of Quaternary Science* 35: 731–736.
- Loucos KE, Simonin KA, Song X, Barbour MM. 2015. Observed relationships between leaf H_2^{18}O Pecllet effective length and leaf hydraulic conductance reflect assumptions in Craig–Gordon model calculations. *Tree Physiology* 35: 16–26.
- Majoube M. 1971. Fractionnement en oxygène 18 et en deutérium entre l'eau et sa vapeur. *Journal de Chimie Physique* 68: 1423–1436.
- Martínez-Sancho E, Treydte K, Lehmann MM, Rigling A, Fonti P. 2022. Drought impacts on tree carbon sequestration and water use – evidence from intra-annual tree-ring characteristics. *New Phytologist* 236: 58–70.
- McCarroll D, Loader NJ. 2004. Stable isotopes in tree rings. *Quaternary Science Reviews* 23: 771–801.
- Miller DL, Mora CI, Grissino-Mayer HD, Mock CJ, Uhle ME, Sharp Z. 2006. Tree-ring isotope records of tropical cyclone activity. *Proceedings of the National Academy of Sciences, USA* 103: 14294–14297.
- Nelson DB, Basler D, Kahmen A. 2021. Precipitation isotope time series predictions from machine learning applied in Europe. *Proceedings of the National Academy of Sciences, USA* 118: e2024107118.
- Offermann C, Ferrio JP, Holst J, Grote R, Siegwolf R, Kayler Z, Gessler A. 2011. The long way down – are carbon and oxygen isotope signals in the tree ring uncoupled from canopy physiological processes? *Tree Physiology* 31: 1088–1102.
- Ogée J, Barbour MM, Wingate L, Bert D, Bosc A, Stievenard M, Lambrot C, Pierre M, Bariac T, Loustau D *et al.* 2009. A single-substrate model to interpret intra-annual stable isotope signals in tree-ring cellulose. *Plant, Cell & Environment* 32: 1071–1090.
- O'Neill MA, York WS. 2018. The composition and structure of plant primary cell walls. In: Roberts JA, ed. *Annual plant reviews online*. Chichester, UK: John Wiley & Sons, 1–54.
- Pérez-de-Lis G, Rathgeber CBK, Fernández-de-Uña L, Ponton S. 2021. Cutting tree rings into time slices: how intra-annual dynamics of wood formation help decipher the space-for-time conversion. *New Phytologist* 233: 1520–1534.
- Peters RL, Balanzategui D, Hurley AG, Arx GV, Prendin AL, Cuny HE, Björklund J, Frank DC, Fonti P. 2018a. RAPTOR: row and position tracheid organizer in R. *Dendrochronologia* 47: 10–16.
- Peters RL, Fonti P, Frank DC, Poyatos R, Pappas C, Kahmen A, Carraro V, Prendin AL, Schneider L, Baltzer JL *et al.* 2018b. Quantification of uncertainties in conifer sap flow measured with the thermal dissipation method. *New Phytologist* 219: 1283–1299.
- R Development Core Team. 2015. *A language and environment for statistical computing*. Vienna, Austria: R Foundation for Statistical Computing.
- Rathgeber CBK, Cuny HE, Fonti P. 2016. Biological basis of tree-ring formation: a crash course. *Frontiers in Plant Science* 7: 1–7.
- Roden J, Kahmen A, Buchmann N, Siegwolf R. 2015. The enigma of effective path length for ^{18}O enrichment in leaf water of conifers: ^{18}O enrichment of conifer leaf water. *Plant, Cell & Environment* 38: 2551–2565.
- Roden JS, Lin G, Ehleringer JR. 2000. A mechanistic model for interpretation of hydrogen and oxygen isotope ratios in tree-ring cellulose. *Geochimica et Cosmochimica Acta* 64: 21–35.
- Rossee Y. 2012. LAVAAN: an R package for structural equation modeling. *Journal of Statistical Software* 48: 1–36.
- Rossi S, Anfodillo T, Menardi R. 2006. TREPOR: a new tool for sampling microcores from tree stems. *IAWA Journal* 27: 89–97.
- Scheidegger Y, Saurer M, Bahn M, Siegwolf R. 2000. Linking stable oxygen and carbon isotopes with stomatal conductance and photosynthetic capacity: a conceptual model. *Oecologia* 125: 350–357.
- Song X, Barbour MM, Farquhar GD, Vann DR, Helliker BR. 2013. Transpiration rate relates to within- and across-species variations in effective path length in a leaf water model of oxygen isotope enrichment: transpiration-related variation in Pécllet path length. *Plant, Cell & Environment* 36: 1338–1351.
- Song X, Farquhar GD, Gessler A, Barbour MM. 2014. Turnover time of the non-structural carbohydrate pool influences $\delta^{18}\text{O}$ of leaf cellulose. *Plant, Cell & Environment* 37: 2500–2507.
- Song X, Lorrey A, Barbour MM. 2022. Environmental, physiological and biochemical processes determining the oxygen isotope ratio of tree-ring cellulose. In: Siegwolf RTW, Brooks JR, Roden J, Saurer M, eds. *Tree physiology. Stable isotopes in tree rings*. Cham, Switzerland: Springer International Publishing, 311–329.
- Sternberg L, DeNiro MJ. 1983. Biogeochemical implications of the isotopic equilibrium fractionation factor between the oxygen atoms of acetone and water. *Geochimica et Cosmochimica Acta* 47: 2271–2274.
- Sternberg L, Ellsworth PFV. 2011. Divergent biochemical fractionation, not convergent temperature, explains cellulose oxygen isotope enrichment across latitudes. *PLoS ONE* 6: e28040.
- Sternberg L, Pinzon MC, Anderson WT, Jahren AH. 2006. Variation in oxygen isotope fractionation during cellulose synthesis: intramolecular and biosynthetic effects. *Plant, Cell & Environment* 29: 1881–1889.
- Szejner P, Clute T, Anderson E, Evans MN, Hu J. 2020. Reduction in lumen area is associated with the $\delta^{18}\text{O}$ exchange between sugars and source water during cellulose synthesis. *New Phytologist* 226: 1583–1593.
- Treydte K, Boda S, Graf Pannatier E, Fonti P, Frank D, Ullrich B, Saurer M, Siegwolf R, Battipaglia G, Werner W *et al.* 2014. Seasonal transfer of oxygen isotopes from precipitation and soil to the tree ring: source water versus needle water enrichment. *New Phytologist* 202: 772–783.
- Treydte K, Frank D, Esper J, Andreu L, Bednarz Z, Berninger F, Boettger T, D'Alessandro CM, Etien N, Filot M *et al.* 2007. Signal strength and climate calibration of a European tree-ring isotope network. *Geophysical Research Letters* 34: 2–7.
- Treydte K, Lehmann MM, Wyczesany T, Pfautsch S. 2021. Radial and axial water movement in adult trees recorded by stable isotope tracing. *Tree Physiology* 41: 2248–2261.
- Treydte KS, Schleser GH, Helle G, Frank DC, Winiger M, Haug GH, Esper J. 2006. The twentieth century was the wettest period in northern Pakistan over the past millennium. *Nature* 440: 1179–1182.
- Vitali V, Klesse S, Weigt R, Treydte K, Frank D, Saurer M, Siegwolf RTW. 2021. High-frequency stable isotope signals in uneven-aged forests as proxy for physiological responses to climate in Central Europe. *Tree Physiology* 41: 2046–2062.
- Waterhouse JS, Switsur VR, Barker AC, Carter AHC, Robertson I. 2002. Oxygen and hydrogen isotope ratios in tree rings: how well do models predict observed values? *Earth and Planetary Science Letters* 201: 421–430.
- Wernicke J, Griebinger J, Hochreuther P, Bräuning A. 2015. Variability of summer humidity during the past 800 years on the eastern Tibetan Plateau inferred from $\delta^{18}\text{O}$ of tree-ring cellulose. *Climate of the Past* 11: 327–337.
- Wickham H. 2009. ggplot2: elegant graphics for data analysis. *Applied Spatial Data Analysis* 784: 785.
- Wood S. 2006. *Generalized additive models: an introduction with R*. Boca Raton, FL, USA: Chapman and Hall/CRC.
- Xu G, Liu X, Hu J, Dorado-Liñán I, Gagen M, Szejner P, Chen T, Trouet V. 2022. Intra-annual tree-ring $\delta^{18}\text{O}$ and $\delta^{13}\text{C}$ reveal a trade-off between isotopic source and humidity in moist environments. *Tree Physiology* 42: 2203–2223.
- Yakir D, DeNiro MJ. 1990. Oxygen and hydrogen isotope fractionation during cellulose metabolism in *Lemna gibba* L. *Plant Physiology* 93: 325–332.

Supporting Information

Additional Supporting Information may be found online in the Supporting Information section at the end of the article.

Fig. S1 Raw tree-ring width measurements for the selected trees for the period 2008–2013.

Fig. S2 Mean kinetics of cell wall formation for both years and study sites.

Fig. S3 Individual changes in $\delta^{18}\text{O}$ for the two study years and sites aligned by ring position and time of cell wall formation.

Fig. S4 Seasonal variations of $\delta^{18}\text{O}$ soil (5 and 60 cm), xylem, and needle water from four individuals of *Larix decidua* growing at two different study sites.

Fig. S5 Boxplots of $\delta^{18}\text{O}$ in xylem and needle water and in cellulose as cell as values of diurnal transpiration.

Fig. S6 Observed isotopic composition and enrichment above xylem water for needle water and tree-ring cellulose $\delta^{18}\text{O}$ against vapor pressure deficit.

Fig. S7 Observed isotopic composition and enrichment above xylem water for needle water and tree-ring cellulose $\delta^{18}\text{O}$ against relative humidity.

Fig. S8 Observed enrichment above xylem water for needle water against the observed enrichment above xylem water for tree-ring cellulose $\delta^{18}\text{O}$.

Fig. S9 Mechanistic modeling of the needle water (δ) for both study sites and years.

Fig. S10 Mechanistic modeling of the needle water (Δ) for both study sites and years.

Fig. S11 Predictive accuracy of the Craig–Gordon and Péclet modification in the fractional difference between predicted ($\Delta^{18}\text{O}_M$) and observed bulk needle water enrichment ($\Delta^{18}\text{O}_I$).

Fig. S12 Relation between the proportion of oxygen exchange (p_{ex}) and relative humidity.

Notes S1 Calculation of cell kinetics (timing and residence times).

Notes S2 Parameters of the needle water modeling.

Table S1 Allometric characteristics of the four selected trees.

Please note: Wiley is not responsible for the content or functionality of any Supporting Information supplied by the authors. Any queries (other than missing material) should be directed to the *New Phytologist* Central Office.